# Manipulation of encapsulated artificial phospholipid membranes using sub-micellar lysolipid concentrations.

Pantelitsa Dimitriou[1], Jin Li[1], William D. Jamieson[2], Johannes J. Schneider[3], Oliver K. Castell[2], David A. Barrow[1].

[1]School of Engineering, Cardiff University, Queen's Buildings, CF24 3AA, Wales, United Kingdom.

[2]School of Pharmacy and Pharmaceutical Sciences, College of Biomedical and Life Sciences, Cardiff University, Redwood Building, Kind Edward VII Avenue, CF10 3NB. Wales. United Kingdom.

[3]Institute of Applied Mathematics and Physics, School of Engineering, Zurich University of Applied Sciences, Technikumstr. 9, 8401 Winterthur, Switzerland

*Pantelitsa Dimitriou, *Jin Li.

**Email:** *dimitrioup@cardiff.ac.uk, *lij40@cardiff.ac.uk.

**Author Contributions:** P.D. and J.L. conceived the research with the assistance of O.K.C. and D.A.B. P.D. performed all the experiment. J.L. contributed to the microfluidic experiments. W.D.J contributed to the fluorescent imaging. J.J.S. contributed to the data analysis. P.D. and J.L wrote the manuscript, with contributions from O.K.C., and D.A.B. All authors discussed the results and commented on the manuscript.

**Competing Interest Statement:** The authors declare no conflict of interest.

**Classification:** Physical Sciences, Engineering.

**Keywords:** droplet microfluidics, 3D printing, droplet interface bilayers, lysolipids, artificial membranes.

## Abstract

Engineered artificial cells often involve phospholipid membranes in the form of vesicles or membrane mimics. Droplet interface bilayers (DIBs) constitute a commonly used membrane mimic within synthetic biology. However, these model membranes have limited accessibility due to their requirement to be surrounded by an oil environment. Here, we demonstrate in-situ bilayer manipulation of submillimeter, free-standing, encapsulated droplet interface bilayers (eDIBs) in hydrogel capsules formed by ready-to-use 3D-printed microfluidic devices. The eDIB capsules were exposed to various concentrations of membrane tension-altering lysophosphatidylcholine (LPC), in order to investigate the interaction of lysolipids with three-dimensional, droplet bilayer networks. Micellar LPC concentrations trigger the bursting of the eDIB droplets, while at concentrations below the critical micelle concentration (CMC), the encapsulated aqueous inner droplet networks endure structural changes, precisely affecting the DIB contact angles and bilayer area. Manipulation of these enclosed, 3D-orchestrated membrane mimics facilitates the exploration of readily accessible compartmentalized artificial cellular machinery. Collectively, the multi-compartmentalized capsules and the lysolipid-mediated membrane modulation introduce a chemical approach to control the properties and mechanics of artificial cellular membranes, as well as the functionalities of artificial cells, toward responsive soft material developments and drug delivery applications.

## Significance Statement

Droplet interface bilayers (DIBs) are established robust artificial membrane mimics, widely employed in molecular, chemical and synthetic biology research fields. One critical characteristic of DIBs is the contact area between the aqueous droplets and the supporting materials. To date, post-processing and control of the DIB contact area has been primarily achieved following mechanical approaches, including fine-tuning of electrodes in contact with the droplets. Herein, we demonstrate non-contact manipulation of artificial cellular membranes of microfluidically formed encapsulated DIBs models, using membrane tension-altering lysolipids. This pivots the research toward the non-invasive study of artificial membrane mechanics and the surface density control of membrane integral proteins. These free-standing, soft capsules can serve as drug delivery platforms with partial self-regulation and active payload release mechanisms, responding to natural lysolipid molecules, for both in-vitro and in-vivo studies.

## Introduction

Droplet interface bilayers (DIBs) are bottom-up, cellular membrane mimicking models for the in-vitro study of membrane constituents and properties (1). DIBs are formed when lipid monolayer-coated aqueous droplets come in contact, forming an artificial lipid bilayer membrane (Fig. 1A). In addition, DIBs formed from an aqueous droplet sitting on a hydrogel substrate (2, 3), can support single molecule imaging for biophysical and biochemical studies (4, 5). The versatility of DIB models enables them to be tailored for different research applications, ranging from the study of transmembrane protein behaviors (2), to cell-free DNA expression (6) and in-vitro tissue culture development (7).

Sophisticated and functional artificial cellular architectures can be constructed using DIBs as building blocks. Multisomes (8), enclose DIB networks within an oil droplet, which can be suspended in air or water (9–11). Various multisome demonstrations have been assembled in liquid-only models (8, 11), although, the encapsulation of DIBs and multisomes within solid substrates (12), or soft hydrogels (13), introduces new research and application possibilities. Encapsulated and stored artificial lipid bilayers in solid and semi-solid substrates, acquire enhanced mechanical resistance, leading to their prolonged stability and extended lifetime (13, 14). Gel encapsulated droplet interface bilayer capsules (eDIBs) (15, 16), depict multi-compartmentalized artificial cell chassis, aiming to imprint cellular functionalities, such as polarization (17). DIB systems are usually made by manual pipetting (18), limiting the production yield rate and structural complexity. Recently, multiphase microfluidic droplet-forming devices have been developed to effectively generate DIBs, multisomes and eDIBs, using stepwise emulsifications methods (8, 15, 17). Droplet-based artificial membrane networks formed by robust and high-throughput microfluidic techniques have been used in molecular sensing (8), cell mimicking (17), and artificial cell membrane studies (15).

The properties of DIB systems are determined by the lipid and oil composition (19), membrane chemistry (20), and droplet network arrangement (17, 21). Bilayer mechanics, tension and capacitance are influenced by the DIB properties (22–24), whereas DIB geometrical parameters, e.g., droplet contact angle and bilayer area, are often controlled to modulate transmembrane protein behaviors (25). In addition, mechanosensitive protein channels rely their activation on the asymmetry across a phospholipid bilayer, which was previously established by various DIB models and their post-assembly manipulation (26–28). Attempts have been made to reduce the concentration of proteins pores and channels within the bilayer, by directly dragging/pulling the droplets using electrodes or pipettes (25, 26, 29). Alternatively, DIB manipulation has been achieved via electrowetting methods (22), or through the incorporation of magnetic particles and exposure to magnetic fields (30). Electrowetting manipulation of DIBs can be limited by electroporation and bilayer rupture (31), while mechanical manipulation can be constrained by the contact and movement of invasive pipettes and electrodes, often resulting to the failure of DIBs. Therefore, artificial cell applications would benefit from non-contact and autonomous control of the DIB contact area.

In this work, we propose a chemical approach to alter the structure of encapsulated DIB networks, in order to directly modulate the properties of artificial cells and allow dynamic response to environmental changes. This concept is demonstrated by formulating eDIBs and observing their interaction with water soluble lysophosphatidylcholine (LPC) for prolonged periods. Lysolipids are single-tailed phospholipids, which have been used as membrane tension-modulating agents in various artificial cell studies (32–34). Triple emulsion eDIB capsules were produced consistently by dual-material, 3D-printed microfluidic devices. We find that at high concentrations and above the critical micellar concentration (CMC), LPC induced rupture of the artificial cell membrane mimics and released the encapsulated aqueous content. At low, sub-micellar concentrations the droplet network endures physical changes, with significant alterations on the contact angle and bilayer area. The addition of LPC provides a facile, contact-eliminating method to control the encapsulated DIBs architectures, towards the modulation of artificial cell behaviors and in situ drug delivery applications.

## Results and Discussion

**Microfluidic production and characterization of eDIBs.** Three, in series droplet-forming microfluidic junctions of alternating materials facilitated the formation of complex emulsions capsules. Thus, the microfluidic production of gel eDIBs was achieved in three distinct steps (Fig. 1A). First, the formation of DIBs was escalated following the lipid-out approach, resulting in a water-in-oil (W/O) emulsion. Subsequent injection of the W/O emulsion into an aqueous phase encourages the encapsulation of the DOPC DIBs in an aqueous medium, in this case liquid alginate. Multilamellar DPPC vesicles were dispersed in alginate as surface tension-lowering agents (35, 36), assisting the formation of W/O/W and hindering the coalescence between miscible phases. Finally, the W/O/W was encapsulated by a divalent-infused nanoemulsion, for further emulsification (W/O/W/O) and simultaneous on-chip gelation.

The microfluidic devices used for the production of eDIBs were fabricated using filaments of Nylon and Cyclin Olefin Copolymer (COC), with print settings that can be found in *SI Appendix, Table S1*. For planar microfluidic devices, the water contact angle is vital for successful and stable emulsion formation. Thus, surface contact angle measurements of 3D-printed Nylon and COC substrates exhibited water contact angles of 46 ° and 78°, respectively (Fig. 1B). Nylon fibers and films have been previously used in digital and paper microfluidics as superamphiphobic and anti-corrosive substrates (37–39), however Nylon is not widely used in droplet-microfluidics or 3D-printed microfluidics, possibly due to its hygroscopic properties (40). Here, the 3D-printed Nylon microfluidic component offered a facile method of producing high-order emulsions. In addition, based on the observations during microfluidic experiments, it appeared that Nylon and COC fused well, since there was no leaking at the site of fusion. Previously reported eDIB models were generated using glass capillary/3D-printed hybrid microfluidic devices (15), or though double emulsion 3D-printed devices (17). To our knowledge, this is the first study to demonstrate monolithic, 3D-printed COC/Nylon microfluidic devices that can generate multi-compartment triple emulsions microgels in a robust approach.

Free-standing eDIB capsules with monodispersed droplets can be produced as shown by the exemplar population plotted in Fig. 1C, with an average diameter of 90 μm ± 1 μm. eDIBs with such small inner aqueous droplet diameter have shown to be notably robust after centrifugation (*SI Appendix, Fig. S1*). Often, 3D-printed micro-scale components can introduce variabilities on the microfluidic channel dimensions (*SI Appendix, Table S2 and Fig. S2*). Thus, across experiments eDIBs were formed at multiple phase flow rate combinations (*SI Appendix, Table S3*). The number and diameter of the encapsulated droplets were controlled by the flow rates of the inner aqueous phase and middle lipid oil phase. For reducing the diameter of the inner droplets, the inner aqueous phase flow rate was decreased, and the lipid-containing oil was increased, and vice versa for increasing the droplets' diameter (Fig. 1D). By doing so, the total flow rate of the system was kept constant. For subsequent experiments the flow rates were manipulated accordingly, in order to enclose droplets with large diameter (> 100 μm) and at a small droplet number (< 10), which would permit improved visualization of the droplet arrangement and DIBs.

**Lysolipid-induced droplet release from eDIBs.** Lysolipids and lysolipid-forming enzymes have been integrated within various artificial cell models toward membrane modulation. Reported lysolipid-mediated demonstrations include, de-novo self-assembly and growth of phospholipid membranes (34, 41), protein pore insertion into artificial membranes due to the lateral pressure profile changes of the bilayer (33, 42) and the construction of thermoresponsive vesicles by reducing the phase transition temperature of lipid vesicles (32). When lysolipids are introduced to one leaflet of a lipid bilayer, the phospholipid composition across the membrane changes, causing the membrane to undergo curvature stresses, ultimately affecting the membrane permeability (43–46). Impacts such as the aforementioned are often subtle and occur at concentrations below the CMC, at which concentration the lysolipids have the propensity to be monomers. On the other hand, lysolipid concentrations higher than the CMC, can cause detrimental effects on living cells such as cell death (47), and can cause synthetic cells to

undergo budding or division (48, 49). Egg lysophosphatidylcholine (LPC) is a water soluble, cone-shaped, single-tailed phospholipid with a headgroup larger than the tail, which tends to form micellar lipid structures with positive curvature (50). LPC has been used to alter the membrane tension and activate mechanosensitive channels in DIB systems (28), increase the permeability of cell membranes for drug uptake studies (46, 51), and facilitating protein pore insertion into bilayers (42).

Here, the LPC lysolipids were introduced to the physiological aqueous environment surrounding the eDIBs and diffused passively to the phospholipid DIB between the inner aqueous droplets and the hydrogel shell (droplet-hydrogel DIB). Prior to imaging, the eDIBs were immobilised at the bottom of a 96-well plate using 1 % w/v agarose, and this was followed by the addition of LPC in buffer at the final concentration of interest (Fig. 2A*)*. The amphiphilic lysolipids diffused to the droplet-hydrogel DIB and at high concentrations the inner droplets leaked completely into the surrounding, leaving an empty oil core (Fig. 2B*)*. This was further analysed in terms of the fluorescent signal drop over time, across a population of eDIB capsules exposed to various LPC molarities. The droplet release profile for each concentration over a period of 14 hours is shown in Fig. 2C. After approximately 3 hours of incubation at 37 °C and constant humidity, the intensity stabilised with negligible reduction for eDIB droplets treated with 0 μM and 1 μM LPC, while the eDIBs treated with 10 μM stabilised only temporarily. Exponential decay of the intensity over time is revealed when Fig. 2C is plotted in the logarithmic scale over time with consistent fluctuations indicated at concentrations of 10 μM and higher (*SI Appendix, Fig. S3*). Fluorescence intensity measurements considered only the area of the DIBs inside the whole construct.

The phosphatidylcholine composition used in this study is dominated by approximately 69 % of 16:0 Lyso PC (information provided by manufacturer), leading to the assumption that the critical micelle concentration (CMC) is close to that of 16:0 Lyso PC ($CMC_{LPC}$). The CMC value is a variable of temperature, pH and salt (52, 53), and the exact $CMC_{LPC}$ was not measured in this study. However, previous literature reported that the $CMC_{LPC}$ value of 16:0 Lyso PC ranges between 4 μM and 8.3 μM, at temperatures spanning from 4 °C to 49 °C (54, 55). Therefore, only the 10 μM concentration introduced to the eDIBs in this study, was considered as a concentration closer to previously reported $CMC_{LPC}$. The implication is that either individual LPC lipid molecules, monomers ($<CMC_{LPC}$), or micelles ($>CMC_{LPC}$) were delivered to the droplet-hydrogel DIB, and interacted with the first outer leaflet of the bilayer. This will alter the curvature of the construct, leading to an asymmetric pressure distribution along the bilayer (56). Higher, micellar concentrations of LPC, can lead to the rupture of a phospholipid membrane construct, as a consequence of the translocation of crowded lysolipids to the second inner leaflet of the bilayer, or due to lysolipid-induced perturbations within the bilayer (46, 57, 58). Similarly, here the droplets treated with equal to or greater than 100 μM LPC were subject to rapid droplet bursting, due to the failure of the droplet-hydrogel DIB membrane. In comparison to lower concentrations, this active release was attributed to the concentrated LPC micelles delivered to the targeted site (droplet-hydrogel DIB) and rapidly induced membrane asymmetry.

The exposure duration of phospholipid bilayers to lysolipids has been reported to enhance the lipid molecular transfer to the opposite leaflet (59). This was evident by a fluorescence increase assay, showing that the 10 μM treated eDIBs underwent an initial droplet-hydrogel DIB failure at a later timepoint (~7 hours), compared to higher concentrations which caused instant membrane failure (*SI Appendix, Fig. S3*). Due to the delayed effects of the 10 μM LPC, we assume that at this concentration the micelle formation is negligible (60). This implies that only lipid monomers are present in the aqueous buffer and that 10 μM is therefore considered as a sub-micellar concentration.

Interestingly, it has been reported that transient pores are formed on phospholipid lamellar bilayers, when lysolipids are introduced (32, 61). Furthermore, the micellar size highly depends on the concentration, where 7-50 μM LPC form micelles of 34 Å radius, whereas this micellar radius doubles at concentrations exceeding 50 μM (62). Consequently, concentrations equal to or higher than 100 μM deliver large micelles, which contribute to the possible pore formation at the bilayer, thus the droplet-hydrogel DIB fails and droplet release into the hydrogel occurs. An earlier

active release study on hydrogel eDIBs demonstrated the synergy between pore-forming peptides, but no control over the organization or DIB adhesion was reported (63).

**The effect of sub-micellar LPC concentrations on droplet displacement and arrangement.** Lysolipid molecules tend to insert and rearrange within a phospholipid bilayer (45). This natural behavior of lipid molecules will then alter the membrane, and eventually the whole construct in place. In living systems, increased levels of lysophosphatidylcholine have been found to be associated with cell death activation and neurological pathologies (64, 65). Engineered artificial constructs that resemble biological cells and membranes, utilize low concentrations of lysolipids, in order to harness membrane asymmetry (28).
The addition of practically sub-micellar LPC concentrations into our artificial cell chassis capsule altered the arrangement of the inner DIBs throughout the incubation period. Vesicle phospholipid bilayer studies have shown that the incorporation of single tailed lipids and surfactants induces changes to the membrane tension and promotes membrane growth (42, 66). Depending on the concentration and incubation duration, the lysolipids can insert the first outer leaflet of a bilayer and at this point the bilayer will be unsteadily enlarged due to phospholipid reorganization (57). Therefore, the presence of sub-micellar concentrations of LPC in our system causes the enlargement of the droplet-hydrogel DIB, affecting the equilibrium of the adhesive bilayer forces (F) of the construct. Generally, the bilayer forces are a result of the van der Waals adhesion (67, 68), between lipid monolayer-coated droplets (69), and have been previously used to study the mechanics and separation of DIBs (23). In gel eDIBs, as this droplet-hydrogel DIB expands, the adhesive bilayer forces ($F_{droplet\text{-}hydrogel}$) dominate over the adhesive bilayer forces at the droplet-droplet DIB ($F_{droplet\text{-}droplet}$), leading to the “pulling” of the droplets toward the hydrogel shell (Fig. 3A). Droplet “pulling” was more explicit in eDIBs treated with 10 μM LPC, as shown in Fig. 3B. We define the “pulling” effect, as the retraction of the droplets away from the center of the oil core, whilst others have defined similar phenomena as “unzipping” (26). eDIBs treated with 1 μM LPC were overall less disturbed with mean square displacement (MSD) similar to 0 μM, while the displacement of the droplets exposed to 10 μM LPC was more apparent (Fig. 3C). After approximately 8 hours of incubation with the lysolipids, the “pulling” effect led to droplet merging for eDIBs treated with 10 μM LPC. In fact, we also observed that the inner droplets would mostly merge between them, but not with hydrogel shell. The delayed droplet shifting and displacement in the presence of 10 μM LPC were attributed to the slow build-up of lysolipid concentration at the droplet-hydrogel DIBs, which evidently led to the reduction of the outer leaflet monolayer tension (70).

**The effect of sub-micellar LPC concentrations on DIB bilayer area and contact angle.** In artificial cell studies with components such as transmembrane pores and channels, the bilayer area and contact angle are vital. This is because these characteristics can influence the amount of protein units inserted into the bilayer (1). In DIB electrophysiological studies, the bilayer area can be manipulated by pushing and pulling the electrodes toward and away from the bilayer (9, 29) or by altering the applied voltage (22). Others have induced liquid volume-assisted pressure changes within the droplets participating in the DIB, therefore manipulating the droplet size and the bilayer area (71).
Due to the three-dimensional micro-architecture of the eDIB capsules, the inner DIB network can be oriented to observe and measure the bilayer area at different droplet interfaces, as shown in Fig. 4A. This enabled the quantification of the horizontal and circular bilayer area of 1 μM treated eDIBs, which decreased approximately in the first 7 hours and then reached a plateau. As mentioned earlier, during lysolipid insertion into the droplet-hydrogel DIB, the bilayer grows and the adhesive bilayer forces dominate the bilayer forces between contacting droplets. At sub-micellar concentrations, these changes will occur at a slow rate (58), as shown by the 1 μM treated eDIBs. The bilayer enlargement was also investigated by electrophysiology recordings within a planar droplet-droplet DIB system, showing the growth of the bilayer area over time when one of the droplets had abundant LPC micelles (*SI Appendix, Fig. S4*). Although the DIB

electrophysiology experiments were conducted for a maximum of 20 minutes, they still confirmed that LPC can enlarge the phospholipid bilayer to which they have access to.

The bilayer area of vertical droplet-droplet DIBs was calculated on the assumption that the droplets on either side of the bilayer were of equal diameter (*SI Appendix, Fig. S5*). Furthermore, Fig. 4B shows the average bilayer area of 1 μM and 10 μM treated DIBs throughout the incubation period. The 10 μM LPC caused the merging of the droplets between 3.5 hours and 8 hours. The adhesive bilayer force between any newly formed droplet and an adjacent droplet increases in magnitude (Fig. 3B), hence the bilayer appears larger. This is also explained by the increased bilayer area at ~ 8 hours in Fig. 4B-i, of eDIBs treated with 10 μM LPC. In an LPC saturated aqueous bath, the LPC can continue to influence the droplet-hydrogel DIB after the first droplet merging, leading once again to the weakening of the droplet-droplet DIB, due to the greater adhesive bilayer forces at the droplet-hydrogel DIB, as reflected by the subsequent bilayer area drop at ~11 hours (*SI Appendix, Fig. S6*).

The contact angle of DIBs typically depends on the droplet diameter, lipids and oil composition, as they can affect the surface tension and consequently the droplet-droplet adhesion (19). The number of droplets enclosed within a volume forming DIBs can also affect the droplet-droplet contact angle (21). In most DIB models, the contact angle of DIBs is manipulated prior to the DIB formation by varying the lipid and oil composition (*SI Appendix, Fig. S7)*. In this study, the contact angle among the inner compartments can be manipulated post-fabrication through the incubation of the eDIBs with sub-micellar LPC concentrations. This is displayed in Fig. 4B-ii, where the mean contact angle between eDIB droplets was measured before the LPC starts to affect the droplet-droplet DIBs to a measurable extent, and at the end of the incubation. In addition to the endpoint contact angle measurements, the contact angle was measured at approximately 9 hours for eDIBs treated with 10 μM LPC, representing a timepoint after the first droplet coalescence.

Overall, we demonstrate the release of the inner compartments of free-standing eDIB capsules using micellar lysolipid concentrations, and sub-micellar concentrations to manipulate the bilayer area and contact angle at a microscale level. The artificial membranes were successfully encapsulated into self-supported eDIB capsules using dual material, 3D-printed droplet microfluidic devices, whilst utilizing lipid vesicles as interfacial tension-reducing particles, hindering the mixing between miscible phases. Phospholipid DPPC vesicles within the alginate phase could have contributed to the formation of a DOPC/DPPC bilayer, following a partial lipid-in and lipid-out DIB formation. Although, in this study we considered a symmetric DOPC bilayer formed at the bilayer interface between droplets, and between any droplet and the hydrogel. For the duration of this LPC treatment, we hypothesize that the LPC molecules introduced to the eDIB system were unable to encounter the droplet-droplet DIB, directly. Therefore, the lysolipids only affect the droplet-hydrogel bilayer, where strong adhesion forces pull the droplets and attenuate the droplet-droplet DIB area. These findings demonstrate an in-situ and automated organization and manipulation of the bilayer area and contact angle of encapsulated droplet-droplet DIBs.

Research in artificial cells and protein reconstitutions can benefit from this LPC non-contact modulation of artificial cellular membranes. In addition, this technology can be applied in a wide range of fields including drug encapsulation and on-demand release for in-vivo or in-vitro drug screening studies, as well as the encapsulation and execution of chemical reactions.

To conclude, the enclosure of DIBs is beneficial for establishing communication between the internal and external environment. While many studies have demonstrated the inclusion of DIBs in aqueous environments using the Teflon wire approach (72), only limited studies have utilised soft hydrogels (73). While both approaches stand as robust models, the incorporation of lysolipids within an artificial system can be an advantageous method for manipulating the interface between two or more reagent-carrying compartments. By employing droplet microfluidic technology and DIB network encapsulation in 3D gels, researchers can benefit from high throughput studies and precision engineering of encapsulated membranes structures.

## Materials and Methods

**Materials.** COC was purchased from Creamelt (Grade 8007, TOPAS) and transparent Nylon was purchased from Ultimaker. Sulforhodamine B and calcein were purchased from Thermofisher, UK. The calcein and sulforhodamine were dissolved in 0.05 M HEPES, 0.15 M KCl in deionised water (buffer) or Phosphate Buffered Saline, PBS (pH 7.4, 1 X, Gibco, UK). Alginic acid sodium salt from brown algae, hexadecane, silicone oil AR20, mineral oil, calcium chloride, HEPES, potassium chloride, 1,2-di-oleoyl-sn-glycero-3-phosphocholine (DOPC), 1,2-dipalmitoyl-sn-glycero-3-phosphocholine (DPPC), Egg lysophosphatidylcholine (LPC), chloroform and SPAN 80 were purchased from Merck.

**3D-printed microfluidic device fabrication and operation.** The microfluidic device was designed using COMSOL Multiphysics (versions 5.6) and fabricated using the Ultimaker S5 Pro Bundle with cyclic olefin copolymer (Creamelt) and Nylon (Ultimaker). The device was sliced using the CURA software with the assigned print settings summarized in *SI Appendix*. All devices after printing were stored with silica gel sachets. Each liquid phase was delivered to the microfluidic device using SGE gas-tight glass syringes loaded onto positive displacement syringe pumps (KD Scientific). The SGE syringes were connected directly to the 3D printed microfluidic inlets using PTFE tubing (O.D. ⌀ = 1.58 mm, I.D. ⌀ = 0.80 mm). Further details regarding the microfluidic device, channel dimensions and flow operation can be found in *SI Appendix*.

**Production of Water-in-Oil-in-Water-in-Oil eDIB capsules (W/O/W/O).** All reagents were purchased from Merck, unless otherwise stated. The inner water phase (WP) consisted of a buffer solution of 0.05 M HEPES, 0.15 M potassium chloride, 200 μM of sulforhodamine B (SulfB) or 70 mM calcein. The middle oil phase (OP) consisted of 12.5 mg/mL 1,2-di-oleoyl-sn-glycero-3-phosphocholine (DOPC) in hexadecane. DOPC was first dispersed in hexadecane following the thin film lipid hydration method. Briefly, the DOPC powder was dissolved in chloroform and evaporated using a gentle nitrogen stream until a thin film of lipids was formed. The DOPC film was subject to a vacuum for at least 30 minutes to evaporate any residual chloroform and then released under nitrogen gas. The shell phase (AP) consisted of 1 % w/v alginate and 0.5 mg/mL 1,2-dipalmitoyl-sn-glycero-3-phosphocholine (DPPC) vesicles in buffer. The DPPC vesicle solution was prepared using the thin film lipid hydration method, following vacuum overnight. The DPPC film was dispersed in the buffer solution, vortexed for 30 seconds and sonicated in a water bath at 55 °C for 15 minutes. The eDIB capsules' oil carrier phase (OC) consisted of a $Ca^{2+}$ - infused mineral oil emulsion, which facilitated the gelation of the alginate shell. This carrier phase was prepared by mixing an aqueous solution of 1 g/mL $CaCl_2$ and mineral oil at 1:9 volume ratio, with 1.2 % SPAN 80 surfactant. The mixture was stirred for at least 10 minutes using a magnetic stirrer and plate, creating a $Ca^{2+}$ - infused nanoemulsion. During experiments, the outlet orifice was slightly submerged in 0.2 M $CaCl_2$.

Small and tightly packed DIBs are associated with increased stability (21), as shown by centrifugation experiments in the *SI Appendix*, although, the microfluidic setup and execution here, aimed at the formation of approximately 1 mm diameter eDIBs, with large water droplet compartments (> 100 μm) segregated by artificial lipid membranes (i.e., DIBs).

**LPC treatment of eDIBs.** eDIB capsules were immobilized with 1 % w/v low temperature melting agarose in wells of a 96-well plate. LPC in buffer was prepared and used appropriately, in order for each well to have final LPC concentration of 1, 10, 100 and 1000 μM. The droplet release was evaluated by monitoring the decrease in the fluorescence of sulfB (200 μM) from the droplets of individual eDIBs or the fluorescence increase in the wells with eDIBs encapsulating quenched calcein (70 mM). Details related to the LPC fluorescence increase assay can be found in the *SI Appendix*.

**Optical and Fluorescence Microscopy of eDIBs.** eDIBs during on-chip emulsification were imaged using Dino Lite edge USB microscope. eDIBs post-production and during the LPC treatment were imaged using EVOS M7000 Imaging System. Imaging associated with the

lysolipid treatment was carried out at 37 °C, where the well plate containing the eDIB capsules was sealed with a tape to prevent evaporation.

**Bilayer area and DIB contact angle measurements.** The bilayer area was measured in three different ways depending on the bilayer orientation and sphericity of the droplets forming the DIB. See *SI Appendix* for full bilayer area calculation. Due to the ability of the inner droplets to maintain their three-dimensionality, the contact angle was simply calculated by measuring the angle between two adjacent inner aqueous droplets using the angle drawing tools on ImageJ (2θ). Before measuring the angle, the contrast of the image was adjusted accordingly, in order to remove any noise around the region of interest. The bilayer area and contact angle of eDIBs produced using 4 mg/mL DOPC in 10 % silicone oil were also measured as reference and comparison to conventionally produced eDIBs (12.5 mg/mL DOPC, 100 % hexadecane).

**Fluorescence and image analysis.** The droplet release in the fluorescence decrease assay was evaluated by monitoring the fluorescence decrease from the aqueous sulfB droplets of individual eDIBs. The droplet release in the fluorescence increase assay was evaluated by monitoring the fluorescence increase of the wells with the eDIBs carrying droplets of quenched calcein (70 mM). Image handling and fluorescence analysis were carried out using ImageJ software. The integrated fluorescent intensity was measured at the timepoint of interest, with the ROI minimized to the area of the fluorescent droplets. The intensity plots show the intensity normalised to the intensity extracted from the control (0 μM LPC) fluorescent droplets in eDIBs. The position and displacement of the droplets was recorded using tracking tools within ImageJ. The eDIB samples were monitored for over 10 hours and the position of the droplets was recorded every 5 minutes.

## Acknowledgments

This work was partially supported and funded by the European Horizon 2020 project ACDC (Artificial Cells with Distributed Cores) under project award number 824060 awarded to D.A.B. and O.K.C. at Cardiff University.

## References

1. M. Allen-Benton, H. E. Findlay, P. J. Booth, Probing membrane protein properties using droplet interface bilayers. *Exp Biol Med (Maywood)* **244**, 709–720 (2019).
2. A. Manafirad, “Single Ion-Channel Analysis in Droplet Interface Bilayer” in *Nanopore Technology: Methods and Protocols*, Methods in Molecular Biology., M. A. V. Fahie, Ed. (Springer US, 2021), pp. 187–195.
3. M. J. T. Senior, *et al.*, Single-molecule tracking of perfringolysin O assembly and membrane insertion uncoupling. *The FEBS Journal* **290**, 428–441 (2023).
4. O. K. Castell, P. M. Dijkman, D. N. Wiseman, A. D. Goddard, Single molecule fluorescence for membrane proteins. *Methods* **147**, 221–228 (2018).
5. C. Parperis, M. I. Wallace, “Chapter Fifteen - Single-molecule imaging of pore-forming toxin dynamics in droplet interface bilayers” in *Methods in Enzymology*, Pore-Forming Toxins., A. P. Heuck, Ed. (Academic Press, 2021), pp. 431–459.
6. M. J. Booth, V. R. Schild, A. D. Graham, S. N. Olof, H. Bayley, Light-activated communication in synthetic tissues. *Science Advances* **2**, e1600056 (2016).
7. L. Zhou, *et al.*, Lipid-Bilayer-Supported 3D Printing of Human Cerebral Cortex Cells Reveals Developmental Interactions. *Advanced Materials* **32**, 2002183 (2020).
8. Y. Elani, X. C. I. Solvas, J. B. Edel, R. V. Law, O. Ces, Microfluidic generation of encapsulated droplet interface bilayer networks (multisomes) and their use as cell-like reactors. *Chem. Commun.* **52**, 5961–5964 (2016).

9. G. Villar, H. Bayley, “Functional Droplet Interface Bilayers” in *Encyclopedia of Biophysics*, G. C. K. Roberts, Ed. (Springer, 2013), pp. 861–868.
10. T. Trantidou, M. S. Friddin, A. Salehi-Reyhani, O. Ces, Y. Elani, Droplet microfluidics for the construction of compartmentalised model membranes. *Lab Chip* **18**, 2488–2509 (2018).
11. I. Cazimoglu, M. J. Booth, H. Bayley, A Lipid-Based Droplet Processor for Parallel Chemical Signals. *ACS Nano* **15**, 20214–20224 (2021).
12. S. A. Sarles, D. J. Leo, Physical encapsulation of droplet interface bilayers for durable, portable biomolecular networks. *Lab Chip* **10**, 710–717 (2010).
13. X. Kang, S. Cheley, A. C. Rice-Ficht, H. Bayley, A Storable Encapsulated Bilayer Chip Containing a Single Protein Nanopore. *J. Am. Chem. Soc.* **129**, 4701–4705 (2007).
14. S. Leptihn, *et al.*, Constructing droplet interface bilayers from the contact of aqueous droplets in oil. *Nat Protoc* **8**, 1048–1057 (2013).
15. D. K. Baxani, *et al.*, Bilayer Networks within a Hydrogel Shell: A Robust Chassis for Artificial Cells and a Platform for Membrane Studies. *Angewandte Chemie International Edition* **55**, 14240–14245 (2016).
16. M. Bayoumi, H. Bayley, G. Maglia, K. T. Sapra, Multi-compartment encapsulation of communicating droplets and droplet networks in hydrogel as a model for artificial cells. *Sci Rep* **7**, 45167 (2017).
17. J. Li, *et al.*, Formation of Polarized, Functional Artificial Cells from Compartmentalized Droplet Networks and Nanomaterials, Using One-Step, Dual-Material 3D-Printed Microfluidics. *Adv Sci (Weinh)* **7**, 1901719 (2019).
18. M. A. Holden, D. Needham, H. Bayley, Functional Bionetworks from Nanoliter Water Droplets. *J. Am. Chem. Soc.* **129**, 8650–8655 (2007).
19. A. Alcinesio, *et al.*, Controlled packing and single-droplet resolution of 3D-printed functional synthetic tissues. *Nat Commun* **11**, 2105 (2020).
20. J. A. Vance, N. K. Devaraj, Membrane Mimetic Chemistry in Artificial Cells. *J. Am. Chem. Soc.* **143**, 8223–8231 (2021).
21. M. M. Makhoul-Mansour, E. C. Freeman, Droplet-Based Membranous Soft Materials. *Langmuir* **37**, 3231–3247 (2021).
22. G. J. Taylor, G. A. Venkatesan, C. Patrick Collier, S. A. Sarles, Direct in situ measurement of specific capacitance, monolayer tension, and bilayer tension in a droplet interface bilayer. *Soft Matter* **11**, 7592–7605 (2015).
23. Y. Huang, V. Chandran Suja, J. Tajuelo, G. G. Fuller, Surface energy and separation mechanics of droplet interface phospholipid bilayers. *Journal of The Royal Society Interface* **18**, 20200860 (2021).
24. Y. Huang, G. G. Fuller, V. Chandran Suja, Physicochemical characteristics of droplet interface bilayers. *Advances in Colloid and Interface Science* **304**, 102666 (2022).
25. L. C. M. Gross, O. K. Castell, M. I. Wallace, Dynamic and Reversible Control of 2D Membrane Protein Concentration in a Droplet Interface Bilayer. *Nano Lett.* **11**, 3324–3328 (2011).
26. J. S. Najem, E. C. Freeman, A. Yasmann, S. Sukharev, D. J. Leo, Mechanics of Droplet Interface Bilayer “Unzipping” Defines the Bandwidth for the Mechanotransduction Response of Reconstituted MscL. *Advanced Materials Interfaces* **4**, 1600805 (2017).

27. K. R. Rosholm, *et al.*, Activation of the mechanosensitive ion channel MscL by mechanical stimulation of supported Droplet-Hydrogel bilayers. *Sci Rep* **7**, 45180 (2017).
28. R. Strutt, *et al.*, Activating mechanosensitive channels embedded in droplet interface bilayers using membrane asymmetry. *Chem Sci* **12**, 2138–2145 (2021).
29. S. Lee, H. Bayley, Reconstruction of the Gram-Negative Bacterial Outer-Membrane Bilayer. *Small* **18**, 2200007 (2022).
30. M. M. Makhoul-Mansour, J. B. El-Beyrouthy, L. Mao, E. C. Freeman, Enhancing membrane-based soft materials with magnetic reconfiguration events. *Sci Rep* **12**, 1703 (2022).
31. J. T. Sengel, M. I. Wallace, Measuring the potential energy barrier to lipid bilayer electroporation. *Philosophical Transactions of the Royal Society B: Biological Sciences* **372**, 20160227 (2017).
32. I. Gispert, *et al.*, Stimuli-responsive vesicles as distributed artificial organelles for bacterial activation. *Proc. Natl. Acad. Sci. U.S.A.* **119**, e2206563119 (2022).
33. J. W. Hindley, *et al.*, Building a synthetic mechanosensitive signaling pathway in compartmentalized artificial cells. *Proc. Natl. Acad. Sci. U.S.A.* **116**, 16711–16716 (2019).
34. M. L. Qualls, R. Sagar, J. Lou, M. D. Best, Demolish and Rebuild: Controlling Lipid Self-Assembly toward Triggered Release and Artificial Cells. *J. Phys. Chem. B* **125**, 12918–12933 (2021).
35. X. Bai, L. Xu, J. Tang, Y. Zuo, G. Hu, Adsorption of Phospholipids at the Air-Water Surface. *Biophysical Journal* **117** (2019).
36. S. Karaz, *et al.*, Multiscale Dynamics of Lipid Vesicles in Polymeric Microenvironment. *Membranes (Basel)* **12**, 640 (2022).
37. T. Gilet, D. Terwagne, N. Vandewalle, Digital microfluidics on a wire. *Appl. Phys. Lett.* **95** (2009).
38. J. Yu, *et al.*, Self-powered droplet manipulation system for microfluidics based on triboelectric nanogenerator harvesting rotary energy. *Lab on a Chip* **21**, 284–295 (2021).
39. L. Jiao, *et al.*, Facile preparation of pliable superamphiphobic papers with high and durable liquid repellency for anti-corrosion and open surface microfluidics. *Applied Surface Science* **606**, 154845 (2022).
40. H. Gong, M. Runzi, Z. Wang, L. Wu, Impact of Moisture Absorption on 3D Printing Nylon Filament in (2022) https:/doi.org/10.26153/tsw/44131 (June 23, 2023).
41. A. Bhattacharya, R. J. Brea, H. Niederholtmeyer, N. K. Devaraj, A minimal biochemical route towards de novo formation of synthetic phospholipid membranes. *Nat Commun* **10**, 300 (2019).
42. C. E. Hilburger, M. L. Jacobs, K. R. Lewis, J. A. Peruzzi, N. P. Kamat, Controlling Secretion in Artificial Cells with a Membrane AND Gate. *ACS Synth. Biol.* **8**, 1224–1230 (2019).
43. D. V. Zhelev, Material Property Characteristics for Lipid Bilayers Containing Lysolipid. *Biophysical Journal* **75**, 321–330 (1998).
44. J. Davidsen, O. G. Mouritsen, K. Jørgensen, Synergistic permeability enhancing effect of lysophospholipids and fatty acids on lipid membranes. *Biochimica et Biophysica Acta (BBA) - Biomembranes* **1564**, 256–262 (2002).
45. J. R. Henriksen, T. L. Andresen, L. N. Feldborg, L. Duelund, J. H. Ipsen, Understanding Detergent Effects on Lipid Membranes: A Model Study of Lysolipids. *Biophysical Journal* **98**, 2199–2205 (2010).

46. A. Arouri, O. G. Mouritsen, Membrane-perturbing effect of fatty acids and lysolipids. *Progress in Lipid Research* **52**, 130–140 (2013).
47. M.-C. Chang, *et al.*, Lysophosphatidylcholine induces cytotoxicity/apoptosis and IL-8 production of human endothelial cells: Related mechanisms. *Oncotarget* **8**, 106177–106189 (2017).
48. T. F. Zhu, J. W. Szostak, Coupled Growth and Division of Model Protocell Membranes. *J. Am. Chem. Soc.* **131**, 5705–5713 (2009).
49. Stephanie J. Zhang, *et al.*, Passive endocytosis in model protocells. *bioRxiv*, 2023.01.07.522792 (2023).
50. S. Zalba, T. L. M. ten Hagen, Cell membrane modulation as adjuvant in cancer therapy. *Cancer Treatment Reviews* **52**, 48–57 (2017).
51. N. Rasmussen, J. H. Andersen, H. Jespersen, O. G. Mouritsen, H. J. Ditzel, Effect of free fatty acids and lysolipids on cellular uptake of doxorubicin in human breast cancer cell lines. *Anti-Cancer Drugs* **21**, 674–677 (2010).
52. G. A. Senisterra, E. A. Disalvo, J. J. Gagliardino, Osmotic dependence of the lysophosphatidylcholine lytic action on liposomes in the gel state. *Biochimica et Biophysica Acta (BBA) - Biomembranes* **941**, 264–270 (1988).
53. N. Baccile, A. Poirier, “Chapter 1 - Microbial bio-based amphiphiles (biosurfactants): General aspects on critical micelle concentration, surface tension, and phase behavior” in *Biosurfactants*, Foundations and Frontiers in Enzymology., G. Soberón-Chávez, Ed. (Academic Press, 2023), pp. 3–31.
54. I. Hara, H. Kaneko, A. Kato, The Critical Micelle Concentration of Phospholipids. *Journal of Japan Oil Chemists' Society* **9**, 407–409 (1960).
55. D. Marsh, *Handbook of Lipid Bilayers, Second Edition* (CRC Press, 2013).
56. S. J. Marrink, A. H. de Vries, D. P. Tieleman, Lipids on the move: Simulations of membrane pores, domains, stalks and curves. *Biochimica et Biophysica Acta (BBA) - Biomembranes* **1788**, 149–168 (2009).
57. D. Needham, N. Stoicheva, D. V. Zhelev, Exchange of monooleoylphosphatidylcholine as monomer and micelle with membranes containing poly(ethylene glycol)-lipid. *Biophys J* **73**, 2615–2629 (1997).
58. L. Hua, M. D. Kaiser, H. H. Heerklotz, Vesicle budding caused by lysolipid-induced asymmetry stress. *Biophysical Journal* **122**, 79a (2023).
59. D. Needham, D. V. Zhelev, Lysolipid exchange with lipid vesicle membranes. *Ann Biomed Eng* **23**, 287–298 (1995).
60. E. A. Disalvo, L. I. Viera, L. S. Bakas, G. A. Senisterra, Lysophospholipids as Natural Molecular Harpoons Sensing Defects at Lipid Membranes. *Journal of Colloid and Interface Science* **178**, 417–425 (1996).
61. J. N. Israelachvili, S. Marčelja, R. G. Horn, Physical principles of membrane organization. *Quart. Rev. Biophys.* **13**, 121–200 (1980).
62. M. E. Haberland, J. A. Reynolds, Interaction of L-alpha-palmitoyl lysophosphatidylcholine with the AI polypeptide of high density lipoprotein. *Journal of Biological Chemistry* **250**, 6636–6639 (1975).
63. D. K. Baxani, W. D. Jamieson, D. A. Barrow, O. K. Castell, Encapsulated droplet interface bilayers as a platform for high-throughput membrane studies. *Soft Matter* **18**, 5089–5096 (2022).
64. T. Schilling, C. Eder, Sodium dependence of lysophosphatidylcholine-induced caspase-1 activity and reactive oxygen species generation. *Immunobiology* **216**, 118–125 (2011).

65. C. Huang, C. Freter, Lipid Metabolism, Apoptosis and Cancer Therapy. *Int J Mol Sci* **16**, 924–949 (2015).
66. D.-W. Jeong, H. Jang, S. Q. Choi, M. C. Choi, Enhanced stability of freestanding lipid bilayer and its stability criteria. *Sci Rep* **6**, 38158 (2016).
67. R. Orozco-Alcaraz, T. L. Kuhl, Interaction Forces between DPPC Bilayers on Glass. *Langmuir* **29**, 337–343 (2013).
68. J. M. Frostad, M. Seth, S. M. Bernasek, L. Gary Leal, Direct measurement of interaction forces between charged multilamellar vesicles†. *Soft Matter* **10**, 7769–7780 (2014).
69. M. Yanagisawa, T. Yoshida, M. Furuta, S. Nakata, M. Tokita, Adhesive force between paired microdroplets coated with lipid monolayers. *Soft Matter* **9**, 5891–5897 (2013).
70. M. Traïkia, D. E. Warschawski, O. Lambert, J.-L. Rigaud, P. F. Devaux, Asymmetrical Membranes and Surface Tension. *Biophysical Journal* **83**, 1443–1454 (2002).
71. E. C. Freeman, J. S. Najem, S. Sukharev, M. K. Philen, D. J. Leo, The mechanoelectrical response of droplet interface bilayer membranes. *Soft Matter* **12**, 3021–3031 (2016).
72. M. J. Booth, I. Cazimoglu, H. Bayley, Controlled deprotection and release of a small molecule from a compartmented synthetic tissue module. *Commun Chem* **2**, 1–8 (2019).
73. P. Hardinge, D. K. Baxani, T. McCloy, J. A. H. Murray, O. K. Castell, Bioluminescent detection of isothermal DNA amplification in microfluidic generated droplets and artificial cells. *Sci Rep* **10**, 21886 (2020).

## Figures

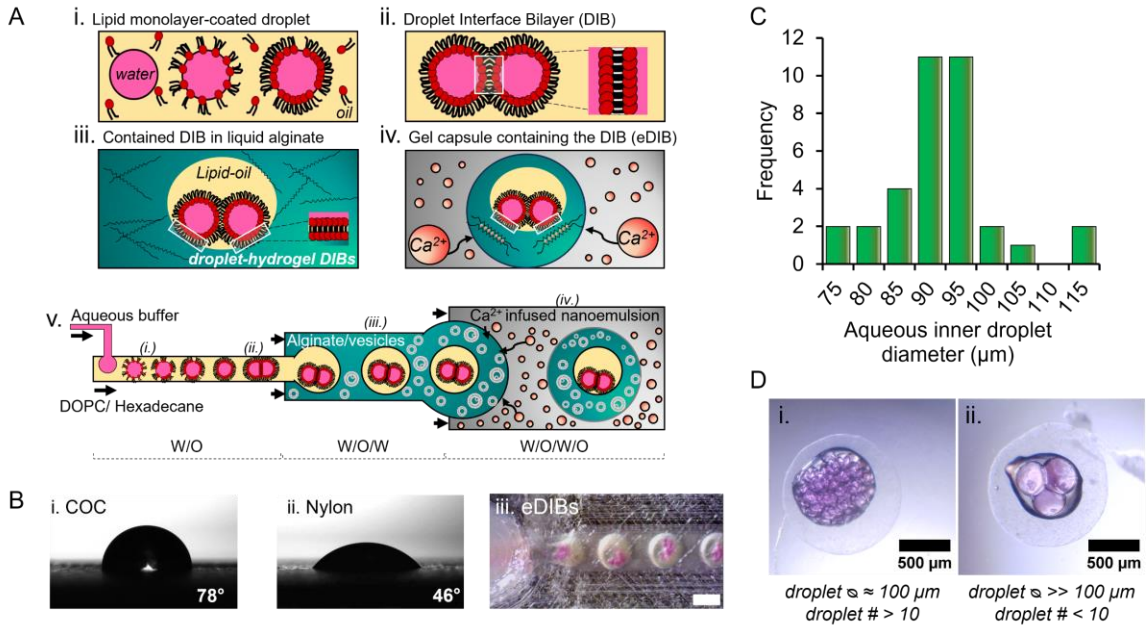


**Fig. 1. Monolithic 3D-printed microfluidic devices yield versatile triple emulsion capsules of encapsulated droplet interface bilayers (eDIBs).** (A) (i.-v.) Schematics showing the procedures of the on-chip microfluidic formation of eDIBs. Droplet interface bilayers are artificial membrane mimics formed when lipid monolayer-coated droplets come in contact. In this microfluidic setup, at an initial droplet-forming junction, (i.). the aqueous buffer phase is broken into droplets by a lipid-containing oil phase (DOPC dispersed in hexadecane oil), forming a water in oil emulsion (W/O). (ii.) When two droplets come in contract, a DIB is formed. (iii.) At a second junction the DIB is contained by an alginate phase with DPPC vesicles forming a W/O/W emulsion (vesicles are not shown in iii. and iv.). Where an inner aqueous droplet contacts the alginate, another DIB is formed defined as a droplet-hydrogel DIB. (iv.) Finally, the contained DIB is engulfed by an immiscible calcium ($Ca^{2+}$) infused nanoemulsion (W/O/W/O), which facilitates the crosslinking of the alginate polymers and the solidification of the eDIB capsules. (B) (i.) The water contact angle of 3D-printed COC is 78 °, whilst (ii.) the water contact angle of 3D-printed Nylon is 46 °, which here are considered as hydrophobic and hydrophilic substrates, respectively. The wetting properties of microfluidics channels are key for stable emulsions, because they keep the flowing liquid from spreading on the channel walls. Successful high-order emulsification is achieved by alternating between materials of opposite wetting properties, as it was demonstrated here for the (iii.) eDIB formation (scale bar: 1 mm). (C) Diameter distribution plot of an eDIB production experiment, showing monodispersed inner aqueous droplet of average diameter 90 μm (n=35). D) eDIB capsules containing (i.) small droplets, or (ii.) large droplets. These capsules were produced using the same microfluidic circuit, but with different flow rate combinations. Flow rates of (i.) and (ii.) were 0.1: 0.5: 5: 8 mL/hour and 0.2: 0.2: 5: 8 mL/hour, respectively and these correspond to the inner aqueous phase: DOPC+hexadecane: alginate+DPPC vesicles: $Ca^{2+}$-infused nanoemulsion. Figure 1D-i. closely relates to the diameter distribution plotted in Figure 1C.

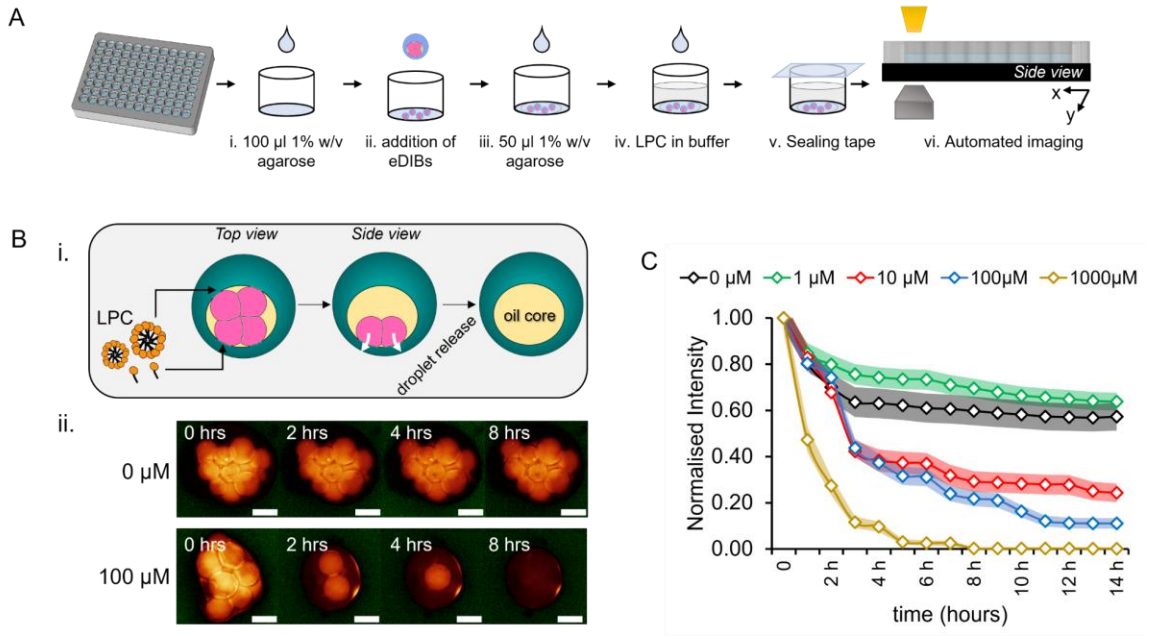


**Fig. 2. The effect of externally added LPC lysolipids on the release of inner aqueous droplet from eDIB capsules.** (A) Stepwise schematic of the LPC treatment execution on eDIB capsules. First, a thin layer of 1 % w/v agarose was added to the well, followed by the addition of eDIB capsules and then another thin layer of agarose. This facilitated the immobilization of eDIBs at the bottom of the plate during the treatment and imaging with the EVOS automated platform. The temperature of the imaging platform was kept at 37 °C and the humidity was controlled by a well plate sealing tape. (B) (i) Top view and side view cartoons of the eDIB capsules, showing the external addition of monomeric and micellar LPC. During the incubation of the eDIBs with concentrated LPC micelles, the lysolipids interact with DIBs formed between the hydrogel and inner aqueous droplets (droplet-hydrogel DIB) and subsequently the droplets get released into the hydrogel. (ii.) Time-lapse of the aqueous fluorescent (sulforhodamine B) inner droplets, showing the rapid release from eDIBs treated with micellar LPC concentrations (100 µM). Scale bar: 200 µm. (C) Fluorescent signal of the eDIB inner droplets incubated with different concentration of LPC (fluorescent decrease assay). The intensity was recorded only within the fluorescent area of the aqueous droplets (when present). The intensity reduction for the untreated eDIB capsules (0 µM) is attributed to artefacts of the automated imaging platform. The sample population per concentration for the intensity analysis was as follows: n= 11 (0 µM), n=15 (1 µM), n=19 (10 µM), n=17 (100 µM), n=16 (1000 µM). The shaded regions for each line plot correspond to the standard error of mean (±SEM).

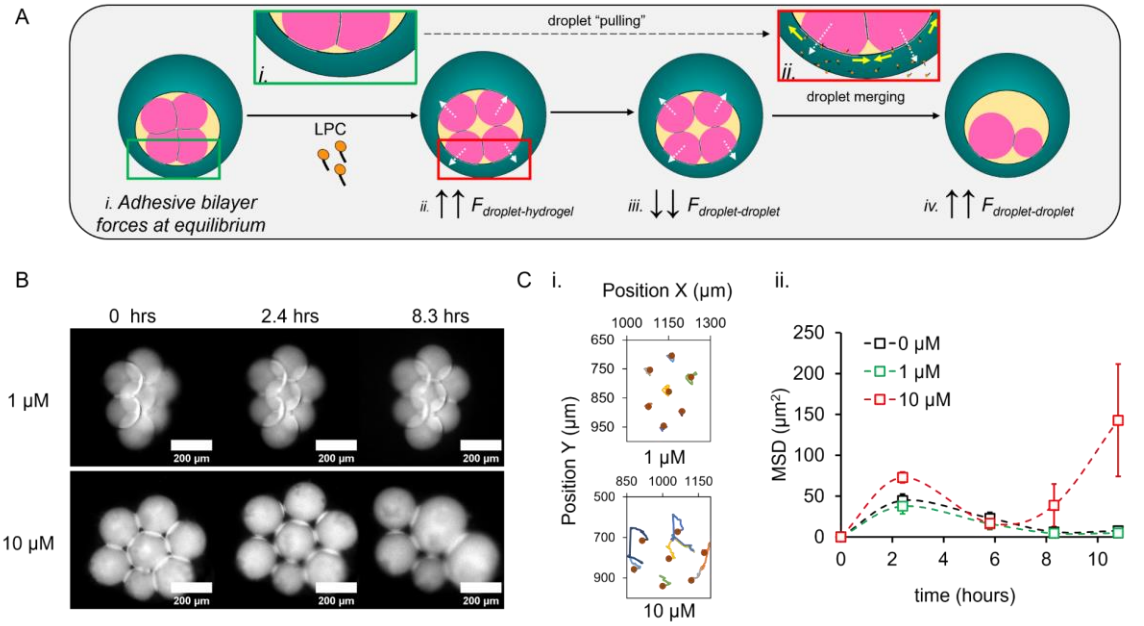


**Fig. 3. Inner droplet re-organization and re-arrangement after incubation with sub-micellar LPC lysolipid concentrations.** (A) Schematic of an eDIB capsule's top view before and after the addition of LPC. (i) Before lysolipid addition the adhesive bilayer forces are at equilibrium, but as the externally introduced LPC acts on the droplet-hydrogel interface, (ii.) the adhesive bilayer forces at the droplet-hydrogel DIBs become greater (↑↑ $F_{droplet\text{-}hydrogel}$) than the droplet-droplet DIB adhesive forces. (iii.) This leads to the weakening of the bilayer adhesion between contacting droplets (↓↓ $F_{droplet\text{-}droplet}$), and the droplets are "pulled" by the dominating forces at the hydrogel interface. The membrane tension is reduced and the bilayer spreads during the insertion of LPC into one leaflet of the droplet-hydrogel DIB, whilst lateral forces introduced at the droplet-hydrogel bilayer (horizontal yellow arrows in magnified schematic ii.), (iv.) lead to the membrane failure and merging of inner droplets. (B) Time lapse of the inner aqueous droplets of eDIBs treated with 1 μM and 10 μM LPC, showing significant "pulling" and subsequent merging of droplets treated with 10 μM LPC. (C) Plots of the (i) X and Y position of the inner droplets and (ii) the mean square displacement of 0 μM, 1 μM and 10 μM LPC treated eDIBs measured over 11 hours, revealing that 1 μM treated droplets travelled similar to the untreated construct, while there was significant travel by 10 μM treated droplets. The dots in (i) show the location of the individual droplets at t=0. Error bars in (ii.) correspond to the standard error of mean (±SEM).

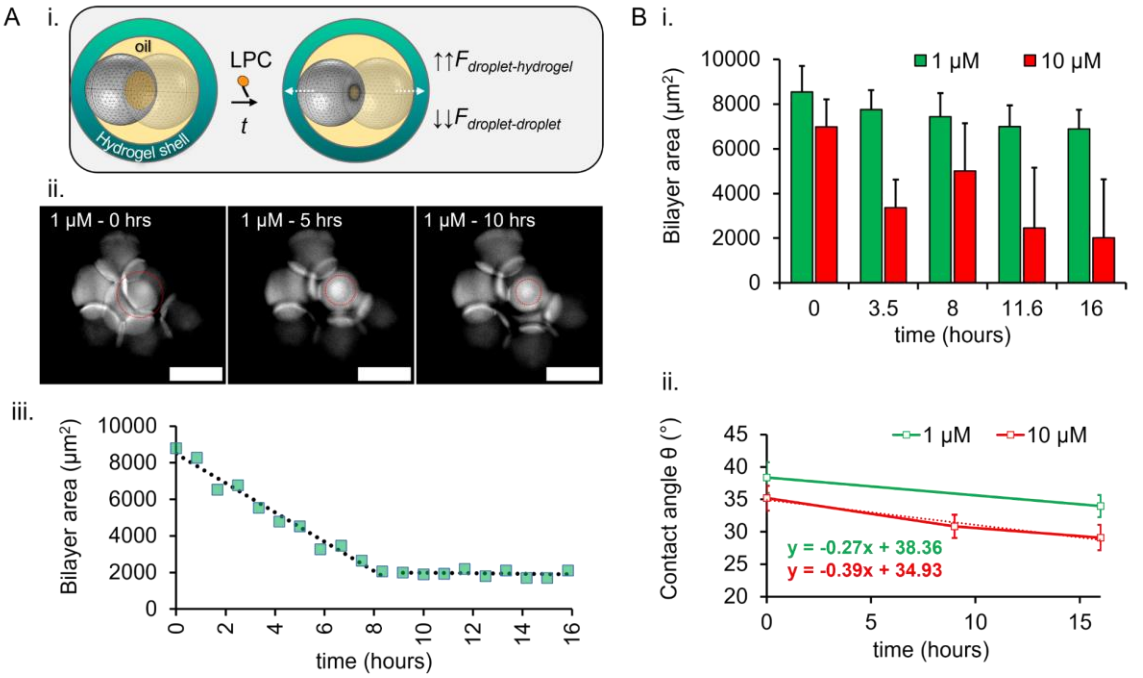


**Fig. 4. LPC lysolipid impact on the bilayer area and contact angle.** (A) (i.) A schematic of an eDIB capsule with two inner droplets and a formed DIB (yellow circular droplet contact area), before and after the addition of LPC. The DIB area is reduced during incubation with LPC, as the adhesive forces of the droplet-hydrogel bilayer (↑↑ $F_{droplet\text{-}hydrogel}$), become greater than the forces of contacting inner droplets (↓↓ $F_{droplet\text{-}droplet}$). (ii.) Time lapse of fluorescent droplets encapsulated within an eDIB capsule treated with 1 μM LPC, showing the reduction of the bilayer area as indicated by the red dotted circle. In order to reveal the bilayer between the contacting droplets, the brightness and contrasts of the image were adjusted. Scale bar: 200 μm. (iii.) The measured circular bilayer area from ii. is plotted over time as a scatter plot, whilst the dotted curve shows the linear decrease in the first 8 hours after 1 μM LPC addition; this is followed by a transition to a constant bilayer area until the end of the study. (B) Plots showing the impact of the sub-micellar concentrations of LPC on the DIB area and contact angle between contacting droplets. (i.) Average DIB bilayer area over time across a population of eDIBs treated with 1 μM (n=11, N=4) and 10 μM (n= 12, N=5) LPC. The DIB bilayer area of 10 μM treated constructs displays a drop at 3.5 hours and then a slight increase at approximately 8 hours, which indicates first the “pulling” of the droplets and subsequent merging, respectively. After that, the bilayer area follows a negligible reduction. On the contrary, 1 μM treated eDIBs did not show any significant or sudden decrease on the bilayer area throughout the study. The number of measured vertical bilayers for 10 μM treated DIBs was initially n= 12 (N=5), but this dropped to n=4 (N=5) by the final timepoint, due to droplet merging. (ii.) Line graph of the average DIB contact angle as a function of time for 1 μM (n =55, N= 6) and 10 μM (n= 47, N=9) treated eDIB capsules. An additional timepoint at approximately 9 hours was plotted, which corresponds to the initial merging of droplets treated with 10 μM (best fit for 10 μM treated eDIBs shown by the dotted line). The line plots are accompanied by linear equations, which reveal the initial average DIB contact angle right after the addition of LPC (38 ° for 1 μM and 35 ° for 10 μM). The population number of the measured contact angles for 10 μM was n=47 (N=9), but this dropped to n=22 (N=9) by the final timepoint, due to droplet merging. The number of eDIBs is noted by N, whilst the sample population of the measurable characteristic (bilayer area or contact angle) is noted by n.